PCCP

PAPER

View Article Online
View Journal | View Issue

Cite this: *Phys. Chem. Chem. Phys.*, 2016, **18**, 17678

Rovibrational energy levels of the $F^-(H_2O)$ and $F^-(D_2O)$ complexes†

János Sarka,[a] David Lauvergnat,*[b] Vincent Brites,[c] Attila G. Császár*[a] and Celine Léonard*[c]

The variational nuclear-motion codes ElVibRot and GENIUSH have been used to compute rotational–vibrational states of the $F^-(H_2O)$ anion and its deuterated isotopologue, $F^-(D_2O)$, employing a full-dimensional, semiglobal potential energy surface (PES) called SLBCL, developed as part of this study for the ground electronic state of the complex. The PES is determined from all-electron, explicitly correlated coupled-cluster singles, doubles, and connected triples [CCSD(T)-F12a] computations with an atom-centered, fixed-exponent Gaussian basis set of cc-pCVTZ-F12 quality. The SLBCL PES accurately reproduces the two equivalent minima of the complex, the corresponding transition barrier of C_{2v} point-group symmetry, as well as the proton transfer and the dissociation asymptotes towards the products HF + OH^- and F^- + H_2O, respectively. The code ElVibRot has been updated so that it can use curvilinear internal coordinates corresponding to a reaction path. The variationally computed vibrational energy levels are compared to relevant experimental and previously determined first-principles results. The vibrational states reveal the presence of pronounced anharmonic effects and considerable intermode couplings resulting in strong resonances, involving in particular the HOH bend and the ionic OH stretch motions. Tunneling results in particularly significant splittings for $F^-(H_2O)$; as expected, the splittings are orders of magnitude smaller for the $F^-(D_2O)$ molecule. The rovibrational energy levels reveal that, despite the large-amplitude vibrational motions, the rotations of $F^-(H_2O)$ basically follow rigid-rotor characteristics.

Received 29th April 2016,
Accepted 7th June 2016

DOI: 10.1039/c6cp02874h

www.rsc.org/pccp

1 Introduction

Among the many questions which can be raised about micro-hydration of small anions, resulting in systems such as $X^-(H_2O)_n$ (X = halogen and n is a small number, perhaps n = 1–4), an extremely interesting one concerns the structure and dynamics of anionic hydrogen bonds. While cationic H-bonds have received a lot of attention, not least due to their role in advanced techniques of mass spectrometry (see ref. 1 and references therein), anionic H-bonds are much less well studied.[2–17]

Due to the large electronegativity and the large proton affinity (PA) of F, the anionic complex $F^-(H_2O)$ is a small but nevertheless intriguing member of the $X^-(H_2O)_n$ cluster family. Thus, a considerable number of experimental and theoretical studies have been performed on this four-atomic complex.[5,7–10,13–16] Three of the six vibrational fundamentals of $F^-(H_2O)$ correspond formally to the "free" H_2O molecule; however, due to the high PA of F^-, the "ionic OH stretching" (iOH) fundamental is considerably different from that characterizing the other halogenated $X^-(H_2O)$ (X = Cl, Br, I) complexes. Furthermore, the overtones and the combination bands of $F^-(H_2O)$ are much more anharmonic and more strongly mixed than those of the other hydrated halogens.

In a series of papers,[7,10,13] details about the mid-infrared (mid-IR) vibrational spectrum of the $F^-(H_2O)$ complex, obtained *via* infrared predissociation (IRPD) spectroscopy of Ar-tagged clusters, have been reported. The increased complexity of the spectrum is due partly to the large anharmonicity of the iOH stretching mode and partly to the delocalization of the negative charge. Links have been made between the shape of the potential and the proton affinity of X in $X^-(H_2O)$.[10] Roscioli *et al.*[10] have demonstrated that the proton-transfer potential becomes flatter with the increase of the basicity of the X^- anion. For $Cl^-(H_2O)$, the proton remains strongly attached to O, whereas the $OH^-(H_2O)$ PES presents a small barrier for the proton exchange. In the case of $F^-(H_2O)$, this motion has been described[7,10,13] as intermediate between a free OH stretch and an intramolecular stretch, as the

[a] *Laboratory of Molecular Structure and Dynamics, Institute of Chemistry, Eötvös University and MTA-ELTE Complex Chemical Systems Research Group, P. O. Box 32, H-1518 Budapest 112, Hungary. E-mail: csaszar@chem.elte.hu*
[b] *Université Paris-Sud, Laboratoire de Chimie Physique, LCP UMR 8000 CNRS, Bât. 349, F-91405 Orsay, France. E-mail: david.lauvergnat@u-psud.fr*
[c] *Université Paris-Est, Laboratoire Modélisation et Simulation Multi Echelle, MSME UMR 8208 CNRS, 5 bd Descartes, F-77454 Marne-la-Vallée, France. E-mail: celine.leonard@univ-paris-est.fr*

† Electronic supplementary information (ESI) available: The parameters of the PES applied and the complete list of the computed vibrational energy levels of $F^-(H_2O)$. See DOI: 10.1039/c6cp02874h

ground and the first excited state of the iOH stretch are respectively below and above the shelf of the 1D potential associated with this proton transfer. A general conclusion[7] of these studies is that the vibrational excitation of the iOH stretch drives the system from a charge-localized ground state to a charge-delocalized configuration in the excited vibrational states. This iOH excitation can also be viewed as an optically driven intracluster proton transfer.

The complex motion of the charge is highlighted by the fact that two dissociation pathways leading to distinct products, $H_2O + F^-$ and $HF + OH^-$, are possible for energies below 20 000 cm^{-1}. (Note that the HF^- + OH asymptote lies more than 45 000 cm^{-1} above the minimum; thus, it has not been considered in this work.) As a consequence, at least two-dimensional vibrational computations, coupling the OF (r_3) and the iOH (r_2) stretches (see Fig. 1), must be employed to recover the energy level structure characterizing the iOH stretching mode.

As to theory, preliminary single-mode treatments proved to be unable to match the complexity of the observed spectrum of $F^-(H_2O)$;[5,8] as expected, the anharmonic energy levels are significantly overestimated for the ionic OH stretching mode, as compared with the available experimental results (*vide infra*), even if the potential is based on accurate CCSD(T) electronic-structure computations. Chaban *et al.*[9] reported the anharmonic vibrational energy levels of the $F^-(H_2O)$ complex based on CCSD(T)/aug-cc-pVTZ *ab initio* computations coupled with a vibrational coupled cluster (VCC)[18] dynamical approach, where the potential is expressed in terms of one- and two-mode couplings. Toffoli *et al.*[14] were the first to include the couplings between all six modes, and they simulated the IR spectrum of the complex. They used a normal mode representation, the 1D part of the PES was computed at the CCSD(T)/aug-cc-pVQZ level of theory and the other parts were determined at the CCSD(T)/aug-cc-pVTZ level. The vibrational energies and intensities were obtained from vibrational self-consistent-field/vibrational configuration interaction (VSCF/VCI) computations involving a dipole moment surface (DMS). Kamarchik *et al.*[16] have recently determined the full six-dimensional PES incorporating the $H_2O + F^-$ dissociation, as well as a DMS, based on CCSD(T)/aug-cc-pVTZ computations. They incorporated in their treatment part of the PES and the dipole moment data computed by Toffoli *et al.*[14] They have also performed VSCF/VCI computations based on normal coordinates and the Eckart–Watson Hamiltonian in order to determine vibrational energies and the IR spectrum of $F^-(H_2O)$ and $F^-(D_2O)$.

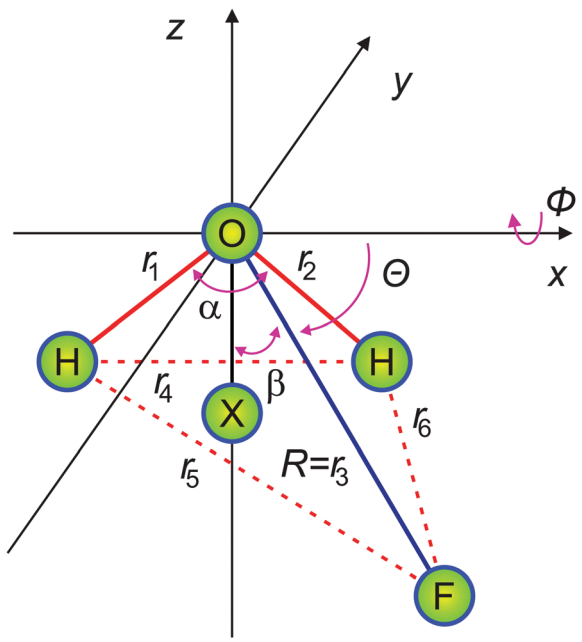

Fig. 1 Definition of the internal coordinates applied during the study of the rovibrational dynamics of the $F^-(H_2O)$ and $F^-(D_2O)$ complexes. The PES is represented in atom–atom distance coordinates $r_1 = R_{OH_1}$, $r_2 = R_{OH_2}$, $r_3 = R_{OF}$, $r_4 = R_{H_1H_2}$, $r_5 = R_{FH_1}$, and $r_6 = R_{FH_2}$. The variational nuclear motion computations utilizing GENIUSH have been carried out using the r_1, r_2, and α valence internal coordinates for the H_2O unit, and the $R = r_3$ and Θ polar coordinates to describe the movement of the fluoride ion in the plane of H_2O. The angles Θ and β can be used to describe the tunneling process. Φ is the out-of-plane angle describing the motion of the F atom with respect to the H_2O plane, which can restrict the fluoride ion "in front of" the water molecule. X denotes a dummy atom.

During the course of the present investigation, a variational study appeared from Wang and Carrington,[17] who used an approach based on curvilinear internal coordinates on a similar system, the $Cl^-(H_2O)$ anion. The computations of Wang and Carrington[17] employed polyspherical coordinates and they compared their accurate results with previous VSCF/VCI computations.[19] They have shown that the energy differences between the two sets of variational vibrational computations employing the same PES are large; for example, for the in-plane wagging fundamental, ν_{ipw}, the difference is as large as 30 cm^{-1}. Furthermore, the tunneling splitting, which cannot be taken properly into account in a standard VSCF/VCI computation, of even the ground vibrational state is as large as 0.4 cm^{-1}.

In summary, most previous first-principles investigations of the dynamics of the $F^-(H_2O)$ system suffered from two shortcomings: the choice of normal coordinates used during the variational nuclear-motion computations and restricted intermode couplings.

The present study was initiated with several goals in mind, the first one being the determination of a full six-dimensional, (semi-)global PES for the $F^-(H_2O)$ complex, covering accurately the regions responsible for the appearance of the low-energy spectra of the anion. A second aim is the determination of the vibrational energy levels of the complex based on variational methods that work in internal coordinates and can cover large regions of the complete PES, thus revealing accurately the dynamics of the system, including tunneling. Third, since the rovibrational energy levels of $F^-(H_2O)$ have not been investigated, accurate computations are performed for them employing the new PES, to ascertain whether these levels show any unusual characteristics as a result of the unusual nuclear dynamics. Two approaches are employed in this study to compute the (ro)vibrational states of the $F^-(H_2O)$ complex and its deuterated analogue, $F^-(D_2O)$: (i) the variational computations with the updated in-house ElVibRot code[20] use a sophisticated

set of curvilinear internal coordinates, suitable to describe and interpret tunneling and large-amplitude internal motions; (ii) the in-house GENIUSH code[21–23] is used for the precise variational computation of the rovibrational energy levels and their characteristics.

2 The SLBCL potential energy surface

The PES of the electronic ground state of the $F^-(H_2O)$ system displays a couple of unusual characteristics. The $F^-(H_2O)$ system has two equivalent C_s minima, separated by a barrier corresponding to a C_{2v} transition state (TS) with a height of around 2500 cm^{-1} (see Fig. 2). There are two important dissociation pathways: they lead towards F^- + H_2O and HF + OH^-, resulting in a highly anharmonic and complex (semi-)global PES.

The choice of the level of electronic structure theory used for the determination of the PES is critical, since it has to be accurate enough to reproduce the complexity of the PES properly and the electronic structure computations should be executed fast enough as a large number of points must be computed. Explicitly correlated methods of electronic structure theory[24,25] appear to be a good compromise, as well demonstrated in the literature.[26–28] The ground electronic state PES of the $F^-(H_2O)$ complex is computed here at the all-electron, explicitly correlated CCSD(T)-F12a level[24,25,29] of electronic structure theory; thus, the important effects of core-valence electron correlation[30] are fully taken into account.

The points of the six-dimensional PES of $F^-(H_2O)$ are generated in this study with the help of the electronic structure code MOLPRO.[31] The computations utilize the atom-centered, fixed-exponent cc-pCVTZ-F12 Gaussian basis set for the F and O atoms and the cc-pVTZ-F12 basis set for H.[32,33] The auxiliary basis sets (ABS) cc-pCVTZ-F12/OPTRI and cc-pVTZ-F12/OPTRI[32,33] are used for the resolution of identity, the aug-cc-pVTZ/JKFIT[34] ABS for the density fitting of the Fock and exchange matrices, and the aug-cc-pwCVTZ/MP2FIT and aug-cc-pVTZ/MP2FIT[34] ABS for the density fitting of the remaining two-electron integrals.

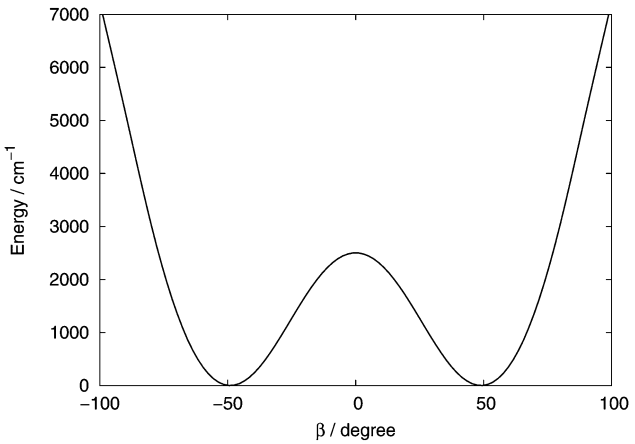

Fig. 2 Minimum-energy path (energy in cm^{-1}) along the angle β (see Fig. 1), showing the C_{2v} transition state and the two equivalent C_s minima characterizing the $F^-(H_2O)$ complex.

All electronic structure computations are performed within the C_1 point group.

22 141 unique points have been computed with an energy not higher than 50 000 cm^{-1} above the minimum, note that the electron affinity of F is 27 431 cm^{-1},[35] and 50 765 further points are generated by symmetry arguments. These points are then fitted by an analytical expression which respects the permutation symmetry of the system, employing a weight function of $0.05/(E + 0.05)$:

$$f(r_1,r_2,r_3,r_4,r_5,r_6) = \sum_{ijklmn} C_{ijklmn} g(r_3)^k g(r_4)^l \times \left(g(r_1)^i g(r_2)^j g(r_5)^m g(r_6)^n + g(r_2)^i g(r_1)^j g(r_6)^m g(r_5)^n \right) \quad (1)$$

with $i + j + k + l + m + n \leq 8$ corresponding to 1107 coefficients (see the ESI†). In eqn (1), $g(r_i) = \exp(-r_i/2.5)$ and the variables r_i correspond to the different distances among the atoms; the coordinate system is illustrated in Fig. 1. The root-mean-square (rms) error of the fit is 7.0 cm^{-1} for energies lower than 10 000 cm^{-1} and 20.0 cm^{-1} for energies higher than this.

The minimum and transition-state geometries of $F^-(H_2O)$ are given in Table 1. The energy barrier between one of the minima and the TS is 2506.4 cm^{-1} at the all-electron cc-pCVTZ-F12 CCSD(T) level, the corresponding value of the fitted PES is 2503.2 cm^{-1}. The minimum and the TS structures are in close agreement with previously computed *ab initio* ones.[16] The minimum-energy path (MEP) connecting the two minima and the TS, based on the PES, is displayed in Fig. 2.

Further one- (1D) and two-dimensional (2D) cuts of the PES are provided in Fig. 3–6. All the notable characteristic features of the PES of the $F^-(H_2O)$ complex are displayed in these figures.

In the 1D iOH cut (see the left panel of Fig. 3), the shoulder lies at about 1500 cm^{-1}. By relaxing the other coordinates, in particular the OF bond length, R, the shelf structure is completely lost (see the right panel of Fig. 3). This shelfless 1D cut can be traced out on the 2D cut representing the OH^- + HF valley, see Fig. 4. The two dissociation pathways in Fig. 4, along the OF and iOH bonds, are well reproduced by the SLBCL PES. The 2D cuts along the angle β and a stretching coordinate (r_2 or R) in Fig. 5 and 6 include the two minima and the TS. In Fig. 5, the two sharp parts of the PES for large values of r_2 illustrate how the F and H atoms avoid each other when the ionic OH bond is stretched. These two structures are linked to dissociation pathways towards

Table 1 Characteristics of the minimum and transition state structures obtained from the analytic representation of the fitted SLBCL PES and from optimizations performed at the *ab initio* all-electron cc-pCVTZ-F12 CCSD(T)-F12a level (see Fig. 1 for the definition of the coordinates, Φ is equal to 90°)

	Minimum (C_s)		Transition state (C_{2v})	
Coordinate	PES	*Ab initio*	PES	*Ab initio*
$r_1 = R_{OH_1}$ (Bohr)	1.808	1.808	1.835	1.835
$r_2 = R_{OH_2}$ (Bohr)	1.982	1.982	1.835	1.835
$r_3 = R_{OF}$ (Bohr)	4.613	4.613	4.829	4.826
α (degree)	102.0	102.1	90.3	90.3
β (degree)	49.0	49.1	0.0	0.0

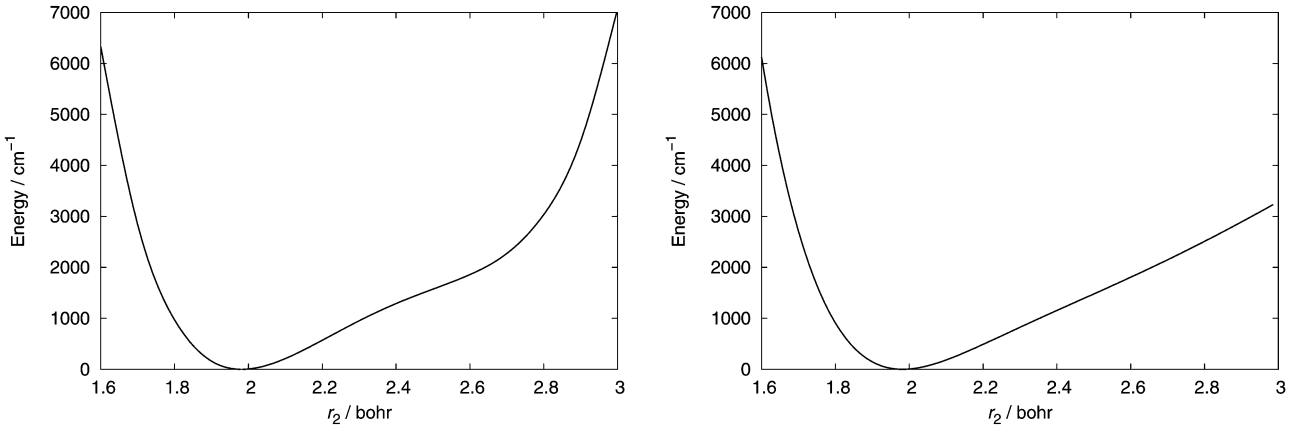

Fig. 3 Left panel: A one-dimensional proton exchange path characterizing the $F^-(H_2O)$ system, obtained after fixing the r_1, α, R, Θ, and Φ coordinates at their equilibrium values. Right panel: Minimum-energy dissociation path of the $F^-(H_2O) \rightarrow HF + OH^-$ reaction along the r_2 coordinate.

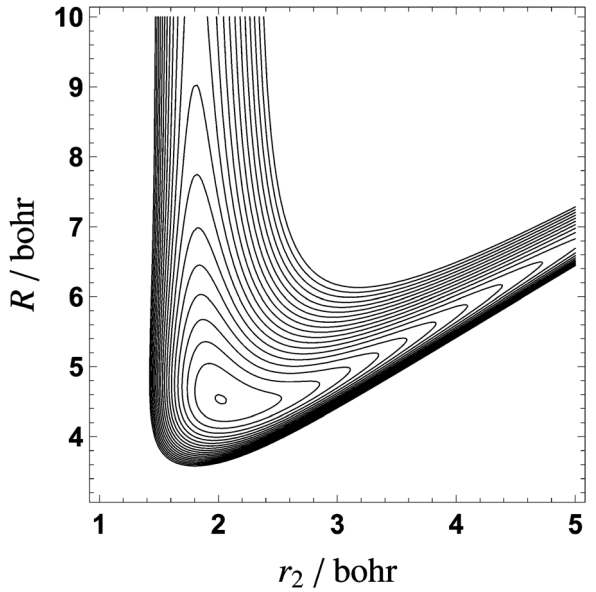

Fig. 4 Two-dimensional cut of the PES along the r_2 and R coordinates. The energy spacing between the adjacent lines is 1000 cm^{-1}. The other internal coordinates are kept fixed at their respective equilibrium values.

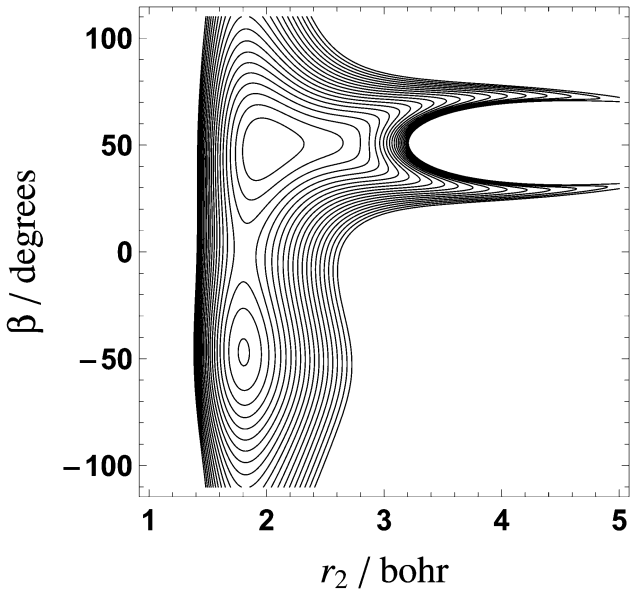

Fig. 5 Two-dimensional cut of the PES along the r_2 and β coordinates. The energy spacing between the adjacent lines is 1000 cm^{-1}. The other internal coordinates are kept fixed at their respective equilibrium values.

OH^- + HF. In Fig. 6, the 2D plots show the variation of the PES with respect to R and β. Comparison of the left and right panels of Fig. 6 helps to visualize the changes arising in the 2D cuts when the other coordinates are fixed at the C_s and the C_{2v} stationary points. One can also notice that it is easier to remove F when it is located along the α bisecting direction than when it is in front of one of the H atoms.

The two coordinates employed in Fig. 4, r_2 and R, describe two dissociation pathways. The corresponding dissociation energies can be computed from the PES and from fragment energies, taking the minimum energy as zero. In what follows, all the coordinates which are not specified are optimized. For the $F^-(H_2O) \rightarrow F^- + H_2O$ reaction, D_e(PES) = 9445 cm^{-1} for r_3 = 50 Bohr, $r_1 = r_2 = R_{OH}$ = 1.807 Bohr, $\alpha = 104.1^\circ$, $\Theta = 90^\circ$, and $\Phi = 90^\circ$, whereas D_e(fragments) = 9633 cm^{-1} with R_{OH} = 1.810 Bohr and $\alpha = 104.5^\circ$. The last value is similar to the one obtained by Kamarchik *et al.*[16] For the $F^-(H_2O) \rightarrow OH^-$ + HF reaction, D_e(PES) = 18 163 cm^{-1} with bond lengths (in Bohr) fixed to r_2 = 10, $r_1 = R_{OH}$ = 1.833, and $r_6 = R_{HF}$ = 1.715, whereas D_e(fragments) = 17 028 cm^{-1} with R_{OH} = 1.821 and R_{HF} = 1.733. The latter reaction can be seen as a Brønsted base hydrolysis reaction due to the high basicity of the F atom.

Table 2 gives the harmonic fundamentals computed both at the equilibrium and the transition-state structures from the PES and *ab initio* calculations. The harmonic wavenumbers obtained in this study agree well with related literature data.[9,16] Table 2 also shows that the ipw, out-of-plane (oop), and iOH modes at the TS are different from their equilibrium counterparts. Thus, anharmonic couplings are expected to play an important role in the dynamics between the relatively soft

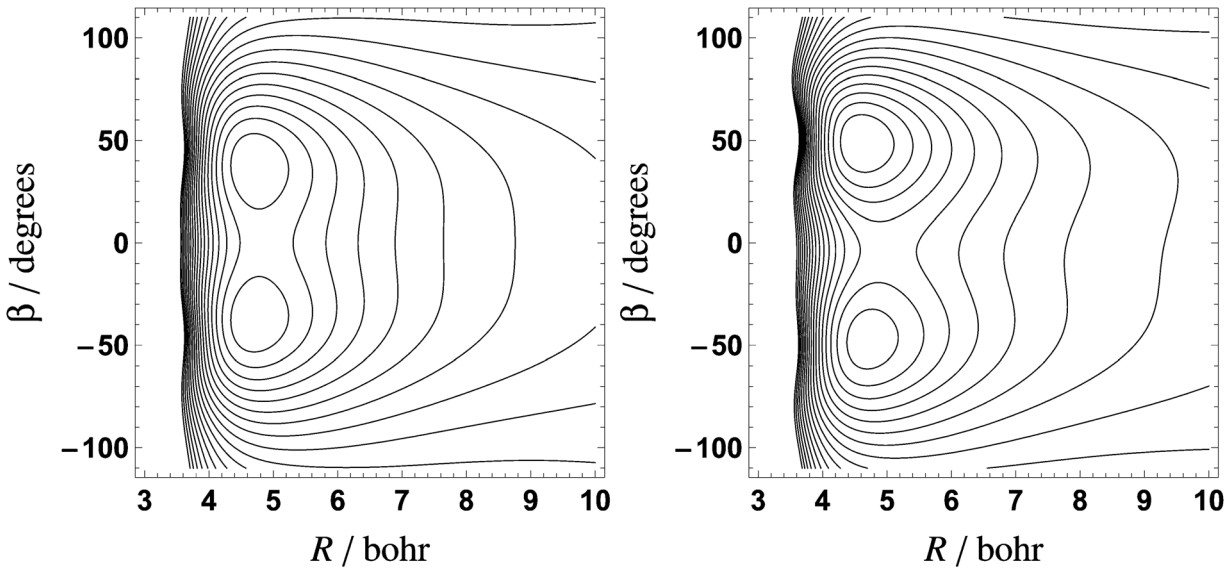

Fig. 6 Two-dimensional cuts of the PES along the R and β coordinates. The energy spacing between the adjacent lines is 1000 cm^{-1}. The other internal coordinates are kept fixed at their respective transition state (left panel) and equilibrium (right panel) values.

Table 2 Harmonic vibrational wavenumbers at the C_s minimum geometry and the C_{2v} transition state obtained from *ab initio* geometry optimizations or from the fitted PES

	Minimum (C_s)			
Characterization	*Ab initio*	PES	Ref. 9[a]	Ref. 16[b]
ω_{iws}: ion-water stretch	384.3	384.7	387	383
ω_{ipw}: in-plane wag	573.6	567.3	580	576
ω_{oop}: out-of-plane bend	1156.2	1156.1	1171	1171
ω_{wb}: HOH bend	1725.9	1716.8	1723	1718
ω_{iOH}: ionic OH stretch	2277.6	2276.6	2211	2205
ω_{fOH}: free OH stretch	3888.6	3886.0	3856	3857
	Transition state (C_{2v})			
Characterization	*Ab initio*	PES	Ref. 16[b]	
ω_{ipw}: in-plane-wag	*i*529.9	*i*527.4	*i*523	
ω_{iws}: ion-water stretch	278.6	277.7	271	
ω_{oop}: out-of-plane bend	850.8	849.7	849	
ω_{wb}: HOH bend	1650.1	1648.9	1611	
ω_{asOH}: asymmetric OH stretch	3689.4	3691.2	3670	
ω_{sOH}: symmetric OH stretch	3739.4	3740.4	3714	

[a] VCC results (CCSD(T)/aug-cc-pVTZ). [b] The PES is based on CCSD(T)/aug-cc-pVTZ computations.

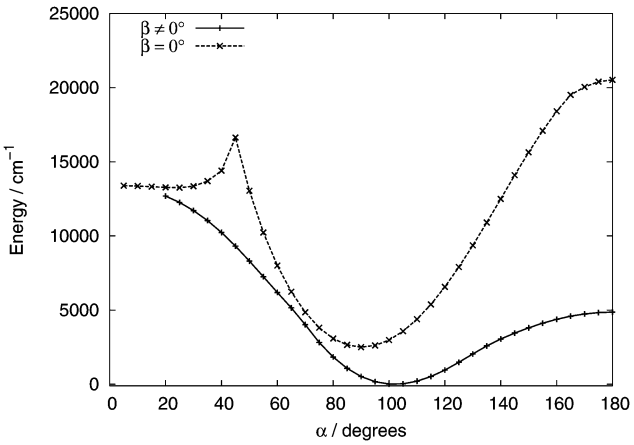

Fig. 7 Minimum energy paths along α for $\beta = 0^\circ$ and relaxed $\beta \neq 0^\circ$. All the other coordinates are free to relax.

ion-molecule motions at the minima and "water" modes at the TS. Discrepancies of about 8 cm^{-1} are observed in the harmonic wavenumbers of the HOH bending and the ipw modes at the equilibrium geometry between the *ab initio* computations and the PES analysis. These differences result from the global 6D fitting process and attest that these modes are influenced by strongly anharmonic parts of the PES. The ipw mode corresponds to a large-amplitude motion between the minima and the transition state, while fitting problems have been encountered for the HOH bending mode (*vide infra*).

Despite our attempts aimed at deriving a fully global PES for $F^-(H_2O)$, certain regions of the present PES should still be considered problematic. In particular, the region associated with $\alpha < 50^\circ$, less important from the point of view of the present dynamical study, is characterized with "holes". This problem could not be corrected and it is associated with the presence of a "bifurcation", shown in Fig. 7 and 8. In Fig. 7, two MEPs along α are presented, one for $\beta = 0^\circ$ and one for relaxed $\beta \neq 0^\circ$. In both cases all the other coordinates are allowed to relax. For geometries where $\beta = 0^\circ$, the F atom lies along the bisector of the α angle.

For α values larger than about 50°, there are no problems with the MEPs shown in Fig. 7. However, for the $\beta = 0^\circ$ MEP, Fig. 7 displays a bifurcation arising when the energy approaches the dissociation energy of the complex at an α value of about 45°. It was checked using EOM-CCSD/aug-cc-pVTZ computations that there are no nearby excited electronic states in this region. At even smaller α angles this MEP "looses its symmetry", due to

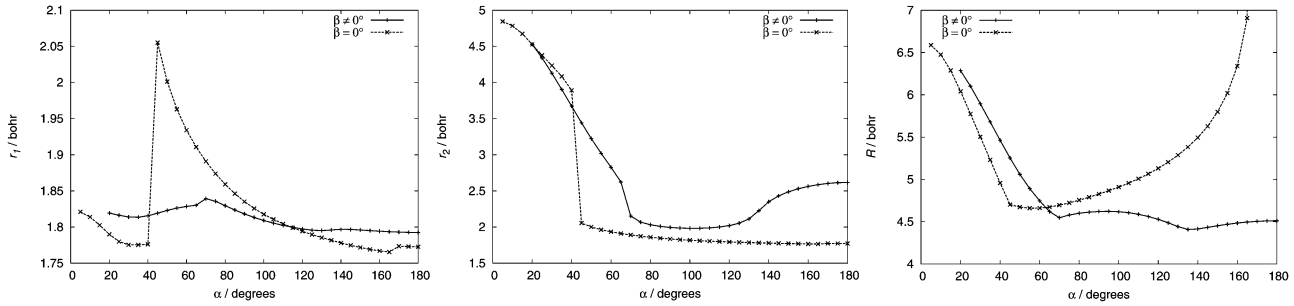

Fig. 8 Variations of r_1 (left), r_2 (middle), and R (right) associated with the minimum-energy path of the PES along α, for the $\beta = 0^\circ$ and relaxed $\beta \neq 0^\circ$ cases.

Table 3 The internal coordinates and the basis sets employed during the final variational computations carried out with GENIUSH; the equilibrium reference geometries and the grid ranges are given in Bohr and degrees for the distance- and angle-type coordinates, respectively. See Fig. 1 for the definition of the internal coordinates[a]

Coord.	DVR type	NBF	EqRG	TSRG[b]	Allowed grid range[c]	Applied grid range[c]
r_1	Laguerre PO-DVR	15	1.80777	1.83462	1.1–3.7	1.41–3.54
r_2	Laguerre PO-DVR	15	1.98240	1.83462	1.1–3.7	1.41–3.54
α	Legendre PO-DVR	15	101.993	90.321	40.0–179.0	49.31–164.40
R	Laguerre PO-DVR	30	4.61388	4.82814	3.7–7.0	3.98–6.93
Θ	Legendre PO-DVR	40	41.0035	90.0	1.0–179.0	4.43–175.57
Φ	Legendre PO-DVR	15	90.0	90.0	1.0–179.0	25.21–154.79

[a] Coord. = coordinate, NBF = number of basis functions, EqRG = equilibrium reference geometry, TSRG = transition state reference geometry, PO = potential optimized, DVR = discrete variable representation. [b] To describe the two equivalent global minimum along Θ, the transition state was used as the reference geometry. [c] Due to the applied PO-DVR, there are differences between the allowed and the actual grid ranges.

the ensuing dissociation to HF + OH^- (see Fig. 8). For $\alpha \leq 20^\circ$, *i.e.*, for the dissociated products, there is seemingly not much difference between the MEPs corresponding to the two choices of β. Nevertheless, the $\beta \neq 0^\circ$ MEP is not drawn below 20° as the PES is not meaningful there. It is difficult to describe regions of the configuration space containing such bifurcations with an analytical function. During the nuclear-motion computations no artificial walls have been utilized to overcome the mentioned drawback of the fitted PES. As a consequence, the range of basis functions describing the HOH bend motion used during the variational nuclear motion computations had to be limited (Table 3, *vide infra*).

Fig. 8 shows the variation of the bond lengths associated with the MEP of the PES along α, for $\beta = 0^\circ$ and relaxed $\beta \neq 0^\circ$. This figure emphasizes the significant changes of the bond lengths when α varies for $\beta = 0^\circ$ and $\beta \neq 0^\circ$. In particular, while one of the OH bond length remains around 2 Bohr along the path, the other OH bond length increases up to 5 Bohr for $\alpha < 50^\circ$. At the same time, the OF bond length increases strongly up to more than 6.5 Bohr for small values of α. Indeed, the molecule tends to have a OH^- + HF configuration in this region. For large values of α, *i.e.*, for $\alpha > 100^\circ$, the variations of OF are different for $\beta = 0^\circ$ and $\beta \neq 0^\circ$. If $\beta = 0^\circ$ and $\alpha \to 180^\circ$, the molecule tends to dissociate towards $H_2O + F^-$, whereas the molecule has a $HOHF^-$ configuration if $\beta \neq 0^\circ$. These strongly asymmetric variations of the OH bond lengths result in holes that can also be observed for large symmetrical elongations of the two OH bonds.

In order to distinguish the present PES from those in the literature, we name the final PES of the present study the SLBCL PES of $F^-(H_2O)$. The PES is completely specified in the ESI.†[36]

3 Rovibrational computations

One of the aims of this study has been the precise determination of the rovibrational energy level structure of the $F^-(H_2O)$ and $F^-(D_2O)$ complexes based on the SLBCL PES. Two approaches and codes have been used for this purpose: ElVibRot and GENIUSH. The use of curvilinear coordinates is known to reduce the computational resources required to perform nuclear-motion computations for floppy molecular systems and to facilitate the precise description of large-amplitude motions and tunneling splittings. The $F^-(H_2O)$ system is characterized by significant coordinate variations along the tunneling motion, described efficiently by the Θ and β coordinates (Fig. 1). Thus, an internal coordinate approach, as used in ElVibRot and GENIUSH, should be preferable over a normal-coordinate-based approach.

The masses of the nuclei used during the variational nuclear motion computations of this study are m_H = 1.00782500 u, m_O = 15.99491926 u, and m_F = 18.99840806 u.

3.1 ElVibRot

In ElVibRot,[20] the time-independent nuclear-motion Schrödinger equation is solved by a numerical approach, whereby TNUM[37] produces the exact kinetic energy operator (KEO) associated with the coordinates required for this study. The ElVibRot program supports the use of coordinate transformations,[38] in the present case from the internal coordinates used in the

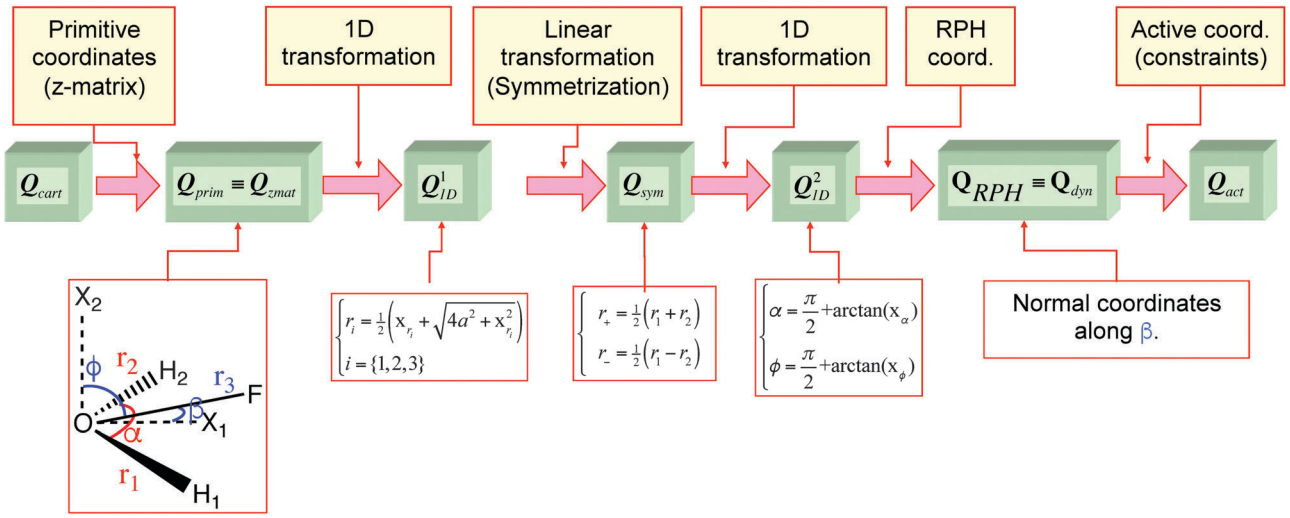

Fig. 9 A scheme describing the coordinate transformations within ElVibRot. The coordinates on the right are the active ones, $\mathbf{Q}_{act}$, used during the dynamical computations, while the coordinates on the left are the Cartesian ones, $\mathbf{Q}_{Cart}$, required in TNUM. X_1 and X_2 correspond to dummy atoms.

dynamical calculation to the Cartesian coordinates needed in the KEO derivation.

To reduce the couplings between modes, we added a new facility to the ElVibRot code so that it can now use complex coordinates similar to the reaction path coordinates within the Reaction Path Hamiltonian (RPH)[39] or the Reaction Surface Hamiltonian (RSH),[40] or more precisely within the approaches developed by Meyer and Günthard[41] and Hougen, Bunker, and Johns (HBJ).[42] To set up RP or MEP coordinates, the following six transformations need to be performed, represented by bold arrows in Fig. 9:

• The first transformation leads from Cartesian coordinates, $\mathbf{Q}_{cart}$, to the primitive curvilinear coordinates defined by means of a Z matrix, $\mathbf{Q}_{ZMAT}$. The first dummy atom, X_1 (see Fig. 9), enables the definition of the angular motion of the F atom with respect to the bisector of the HOH angle. The second dummy atom, X_2, enables to define the polar angle as Φ and the azimuthal angle as β (see Fig. 9). Hence the poles of these two spherical angles are along the OX_2 direction and not along the bisector of HOH (OX_1). At this point it is important to emphasize that the primitive coordinates used with ElVibRot are slightly different from the ones used in GENIUSH. In GENIUSH, their analytical expressions must be available to obtain the KEO, while in ElVibRot, those primitive coordinates are defined with a Z matrix without explicit analytical expressions, as in electronic structure codes.

• The second transformation is just a 1D transformation of the three distances (r_1, r_2, and $r_3 = R$), such that $r_i = 1/2\left(x_{r_i} + \sqrt{(4a^2 + x_{r_i}{}^2)}\right)$ with $i = 1, 2, 3$ and $a = 0.2$. This expression gives almost a straight line ($r_i = x_{r_i}$) when $x_{r_i} > 1$ and it is always positive. Therefore, it enables to change the usual distance range, $]0,\infty[$, to a new range $]-\infty,\infty[$, so that one can use the usual harmonic oscillator (HO) basis in x_{r_i} without reaching negative values of r_i.

• The third transformation enables us to symmetrize the two OH stretch coordinates, although this is not essential. Nevertheless, the Hamiltonian parameters required for the RPH can be adjusted more easily along the path when symmetrized coordinates are used.

• The fourth transformation is another 1D transformation, now of the valence angles α and Φ, such that $\alpha = \pi/2 + \arctan(x_\alpha)$ and $\Phi = \pi/2 + \arctan(x_\Phi)$. The range of the new coordinates, x_α and x_Φ, is infinite in both directions. This transformation enables to push away the numerical singularities when the water molecule is linear ($\alpha = \pi$) or when the F atom reaches the poles.

• The fifth transformation facilitates the use of a RPH and is added to reduce the coupling between the inactive modes. In our implementation, the $\mathbf{Q}_{RPH}$ coordinates are obtained such that the harmonic Hamiltonian contribution (eqn (2)) of the exact Hamiltonian in $\mathbf{Q}_{1D}$ (the coordinates from the previous transformation) along the coordinates of the path becomes an uncoupled harmonic Hamiltonian in $\mathbf{Q}_{RPH}$ (eqn (3)):

$$\hat{H}^{\text{harm}}_{\mathbf{Q}_{1D}}(\mathbf{Q}_{1D};\beta) = \frac{1}{2}\sum_{i=2,j=2}^{6,6} -G^{i,j}(\beta)\frac{\partial^2}{\partial Q^i_{1D} Q^j_{1D}} + h^{i,j}(\beta)\cdot\left(Q^i_{1D} - Q^{Op,i}_{1D}(\beta)\right)\cdot\left(Q^j_{1D} - Q^{Op,j}_{1D}(\beta)\right) \quad (2)$$

where $h^{i,j}(\beta)$, and $G^{i,j}(\beta)$ are, respectively, the elements of the Hessian, and the contravariant components of the metric tensor along the MEP. The $Q^{Op,i}_{1D}(\beta)$ are the optimized geometrical parameters along the MEP and they are obtained by a numerical minimization of the analytical PES. The $h^{i,j}(\beta)$ are obtained with the help of a finite-difference scheme. The Hessian and the optimized geometrical parameters have been fitted using $\cos(m\beta)$ for even functions ($m = [0, 1,\ldots, 5]$) or $\sin(m\beta)$ for odd functions ($m = [1, 2,\ldots, 6]$) and 31 points are used along the 1D path ($\beta = [-1.5, -1.1,\ldots, 1.5]$ rad).

Furthermore,

$$\hat{H}^{\mathrm{harm}}_{\mathbf{Q}_{\mathrm{RPH}}}(\mathbf{Q}_{\mathrm{RPH}};\beta) = \sum_{i=2}^{6} \frac{1}{2}\omega^i(\beta)\left(-\frac{\partial^2}{\partial {Q_{\mathrm{RPH}}}^{i2}} + {Q_{\mathrm{RPH}}}^{i2}\right), \quad (3)$$

and the new coordinates are defined as follows:

$$\mathbf{Q}_{\mathrm{RPH}} = \mathbf{L}(\beta)\cdot(\mathbf{Q}_{1\mathrm{D}} - \mathbf{Q}^{\mathrm{Op}}_{1\mathrm{D}}(\beta)), \quad (4)$$

where $\mathbf{L}(\beta)$ is a matrix containing the normal coordinates along the 1D path and $\mathbf{Q}^{\mathrm{Op}}_{1\mathrm{D}}(\beta)$ is the vector associated to the optimized geometrical parameters $\mathbf{Q}^{\mathrm{Op},i}_{1\mathrm{D}}(\beta)$. The $\mathbf{L}$ matrix is obtained numerically from a procedure[43,44] equivalent to the El'yashevich–Wilson GF matrix approach.[45] With this transformation, we can take into account properly the strong variation of the wavenumbers, $\omega^i(\beta)$, along the 1D path. These wavenumbers are 386, 1155, 1697, 2264 and 3889 cm^{-1} at the minimum, while they are 276, 844, 1645, 3688 and 3747 cm^{-1} at the TS. The five frequencies mentioned are associated, respectively, with the following modes: the F^-H_2O stretch, the out-of-plane motion, the HOH bend, the iOH stretch, and the free OH stretch. The values at the minima and the TS agree well with their *ab initio* counterparts (see Table 2).

• The last transformation of Fig. 9 enables us to set up constraints (like rigid coordinates) and thus to define the active and inactive coordinates. In the present study, this feature is used to define the 1D contracted basis set associated with β, the tunneling coordinate.

While the fifth transformation is not essential to preserve symmetry, it enables the use of a more compact basis set. The ensuing vibrational computations using ElVibRot are relatively standard, the wavefunctions are expanded in a basis set and the corresponding Hamiltonian is diagonalized directly or with the block-Davidson[46,47] scheme when the size of the basis set is large. The global 6D basis set is defined as a direct product of the following two elements. A 1D basis is associated with the tunneling angle β defined as a set of 60 sine functions in the range $\beta \in [-1.7,1.7]$ rad with 100 grid points adapted to this basis set. Furthermore, this basis set is contracted with the help of a 1D model to form a basis set with 40 basis functions. A 5D basis is associated with all the coordinates except the β angle. The basis functions are defined as a product of five HO basis functions. The number of 1D basis functions along each coordinate, nb_i, is defined in terms of a parameter ℓ_i such that $nb_i = 1 + \omega_i\ell_i$ ($\omega_i = 3$, $\ell_i \geq 0$). Furthermore, the ℓ_i are defined such that $\sum_{i=2}^{6} \ell_i \leq L_{\mathrm{B}}$, where the parameter L_{B} enables to define the size of the basis set (with $L_{\mathrm{B}} = 7$ and $L_{\mathrm{B}} = 8$, we have 30 724 and 59 719 5D basis functions, respectively). This non-direct product basis set is equivalent to the pruned basis set of Dawes and Carrington.[48] With this basis set, a Smolyak sparse grid[38,49–51] can be used. The size of the grid is defined with the help of a Smolyak parameter, L_{G}, which has to be larger than or equal to L_{B}. In the current study, L_{G} is defined as $L_{\mathrm{G}} = L_{\mathrm{B}} + 1$ (with $L_{\mathrm{G}} = 8$ and $L_{\mathrm{G}} = 9$ the number of grid point are 886 564 and 2 213 329, respectively).

3.2 GENIUSH

GENIUSH[21,22] is a fourth-age[52] quantum chemical algorithm and code. The acronym GENIUSH stands for general (GE) rovibrational code with numerical (N), internal-coordinate (I), user-specified (US) Hamiltonians (H). In GENIUSH, the Hamiltonian can be written in arbitrary curvilinear internal coordinates and the representations of both the kinetic and the potential energy operators are computed numerically, utilizing the discrete variable representation (DVR).[53] Computation of the required eigenstates is carried out using different implementations of the iterative Lanczos algorithm.[54]

Within the GENIUSH approach the choice of the internal coordinates is of prime importance as convergence of the solution of the nuclear Schödinger equation greatly depends on them and the associated basis functions. The internal coordinates chosen are as follows (see Fig. 1): two stretching coordinates (r_1 and r_2) and a bending coordinate (α) describe the motions of the water molecule, a stretching coordinate (R) and two bending coordinates (Θ and Φ) describe the motions of the fluorine atom, where R is the O–F distance, Θ describes the in-plane bending motion of F in the xz-plane, and Φ describes the out-of-plane motion of F. To define the orientation of the molecule in space, the Eckart embedding is employed.[23] The most important characteristics of the computations carried out with GENIUSH are given in Table 3.

In GENIUSH, analyzing the wave function and labeling of the vibrational states is possible using several techniques. First, expectation values of the coordinates, $\langle q \rangle$ and $\sqrt{\langle q^2 \rangle}$, can be computed and the values of the vibrationally excited states can be compared to the ground state. The differences determine the extent of the excitation along the different coordinates. Second, 2D cuts of the full-dimensional wave function can be produced freezing the other coordinates at a single value (preferably at the minimum or the transition-state geometry). The DVR coefficients in 2D can be plotted and the nodes of the wave function can be determined, which also indicates the extent of the excitation along the different coordinates.

4 Results and discussion

The final results of the variational nuclear motion computations performed with the GENIUSH code are given in Tables 4 and 5 for $F^-(H_2O)$, and in Table 6 for $F^-(D_2O)$. All of the computed vibrational eigenvalues of $F^-(H_2O)$ are given in Table S1 in the ESI.†[36] The variationally computed energy levels reported are converged, the uncertainty of the first 100 eigenvalues is estimated to be less than 0.01 cm^{-1}. The very small tunneling splittings of the zero-point vibration and several lower-lying vibrational states of both species also indicates very small uncertainties in the computed energy levels.

For $F^-(H_2O)$, 300 vibrational eigenvalues were computed, see Table S1 (ESI†) for details, including all of the vibrational fundamentals. The first 110 eigenvalues have been successfully assigned as well as several higher-lying states up to the 200th one (see Tables 4 and 5 for details). For $F^-(D_2O)$, 100 vibrational eigenvalues were computed and assigned (see Table 6).

Table 4 The vibrational energy levels of $F^-(H_2O)$ complex and the tunneling splittings of the formally degenerate pairs. The splitting is defined as the difference between the antisymmetric and symmetric state energy levels, $E_{antisym} - E_{sym}$. All values are in cm^{-1}

No.	Label	Energy	Splitting
1	ZPVE	4831.0	7.7×10^{-7}
3	ν_{iws}	423.5	1.2×10^{-5}
5	ν_{ipw}	560.7	1.7×10^{-4}
7	$2\nu_{iws}$	823.2	5.9×10^{-5}
9	$\nu_{iws} + \nu_{ipw}$	972.3	1.5×10^{-3}
11	$2\nu_{ipw}$	1110.4	8.0×10^{-3}
13	ν_{oop}	1180.7	1.9×10^{-5}
15	$3\nu_{iws}$	1203.7	2.7×10^{-4}
17	$2\nu_{iws} + \nu_{ipw}$	1360.5	6.3×10^{-3}
19	ν_{iOH}	1477.9	8.2×10^{-3}
21	$\nu_{iws} + 2\nu_{ipw}$	1509.6	0.054
23	$\nu_{iws} + \nu_{oop}$	1570.5	1.1×10^{-4}
25	$4\nu_{iws}$	1571.5	2.7×10^{-3}
27	ν_{wb}	1634.4	0.069
29	$3\nu_{ipw}$	1650.5	0.12
31	$3\nu_{iws} + \nu_{ipw}$	1732.4	0.027
33	$\nu_{ipw} + \nu_{oop}$	1735.7	1.4×10^{-3}
35	$2\nu_{iws} + 2\nu_{ipw}$	1879.1	0.28
37	$5\nu_{iws}$	1915.0	0.016
39	$2\nu_{iws} + \nu_{oop}$	1942.7	3.9×10^{-4}
41	$\nu_{iws} + 3\nu_{ipw}$	2009.8	1.2
43	$\nu_{iws} + \nu_{iOH}$	2020.3	0.077
45	$\nu_{ipw} + \nu_{iOH}$	2054.0	0.23
47	$\nu_{iws} + \nu_{wb}$	2075.7	0.12
49	$4\nu_{iws} + \nu_{ipw}$	2110.9	0.11
51	$\nu_{iws} + \nu_{ipw} + \nu_{oop}$	2112.0	9.0×10^{-3}
53	$4\nu_{ipw}$	2149.3	2.2
55	$2\nu_{ipw} + \nu_{iOH}$	2188.1	0.53
57	$3\nu_{iws} + 2\nu_{ipw}$	2236.8	0.92
59	$6\nu_{iws}$	2257.9	0.33
61	$2\nu_{ipw} + \nu_{oop}$	2276.3	0.047
63	$3\nu_{iws} + \nu_{oop}$	2299.1	3.8×10^{-3}
65	$2\nu_{oop}$	2332.2	3.0×10^{-3}
67	$2\nu_{iws} + 3\nu_{ipw}$	2367.0	7.1
69	$5\nu_{iws} + 1\nu_{ipw}$	2420.3	1.1
71	$2\nu_{iws} + \nu_{wb}$	2461.0	0.41
73	$2\nu_{iws} + \nu_{ipw} + \nu_{oop}$	2472.1	0.035
75	$\nu_{iws} + 4\nu_{ipw}$	2484.9	18.3
77	$2\nu_{iws} + \nu_{iOH}$	2546.0	0.68
79	$4\nu_{iws} + 2\nu_{ipw}$	2560.7	1.5

Table 5 The vibrational energy levels of the $F^-(H_2O)$ complex and the tunneling splittings of the formally degenerate pairs. The splitting is defined as the difference between the antisymmetric and symmetric state energy levels, $E_{antisym} - E_{sym}$. All values are in cm^{-1}

No.	Label	Energy	Splitting
81	$7\nu_{iws}$	2566.0	1.0
83	$3\nu_{ipw} + \nu_{iOH}$	2598.3	2.9
85	$3\nu_{iws} + \nu_{iOH}$	2613.8	1.8
87	$\nu_{oop} + \nu_{iOH}$	2621.5	6.0×10^{-3}
89	$5\nu_{ipw}$	2622.7	12.3
90	$\nu_{iws} + 2\nu_{ipw} + \nu_{oop}$	2632.5	0.28
93	$\nu_{iws} + 2\nu_{ipw} + \nu_{iOH}$	2640.6	9.4
95	$4\nu_{iws} + \nu_{oop}$	2657.3	0.062
97	$3\nu_{iws} + 3\nu_{ipw}$	2688.1	15.9
99	$\nu_{iws} + 2\nu_{oop}$	2708.5	0.18
101	$3\nu_{ipw} + \nu_{wb}$	2721.0	7.6
103	$6\nu_{iws} + \nu_{ipw}$	2752.8	6.8
105	$2\nu_{iws} + 4\nu_{ipw}$	2791.2	48.9
106	$3\nu_{ipw} + \nu_{oop}$	2794.6	0.85
108	$3\nu_{iws} + \nu_{ipw} + \nu_{oop}$	2817.9	0.30
110	$2\nu_{iOH}$	2837.3	0.060
115	$\nu_{wb} + \nu_{oop}$	2858.1	0.024
117	$8\nu_{iws}$	2878.8	3.0
119	$\nu_{ipw} + 2\nu_{oop}$	2885.4	0.062
121	$5\nu_{iws} + 2\nu_{ipw}$	2893.9	15.9
124	$5\nu_{iws} + \nu_{oop}$	2963.1	0.14
130	$2\nu_{iws} + 2\nu_{ipw} + \nu_{oop}$	2982.4	1.3
134	$2\nu_{iws} + 2\nu_{oop}$	3020.0	1.6×10^{-3}
138	$7\nu_{iws} + \nu_{ipw}$	3054.6	3.0
144	$5\nu_{iws} + 3\nu_{ipw}$	3109.8	0.95
146	$\nu_{iws} + 3\nu_{ipw} + \nu_{oop}$	3125.4	5.4
150	$\nu_{ipw} + \nu_{iOH} + \nu_{oop}$	3145.0	1.5
152	$\nu_{iws} + \nu_{iOH} + \nu_{oop}$	3151.3	0.50
162	$\nu_{iws} + \nu_{wb} + \nu_{oop}$	3206.5	0.41
166	$2\nu_{wb}$	3213.4	2.58
172	$4\nu_{iws} + \nu_{ipw} + \nu_{oop}$	3262.7	0.24
176	$4\nu_{ipw} + \nu_{oop}$	3278.8	3.3
178	$6\nu_{iws} + \nu_{oop}$	3286.7	8.8
183	$3\nu_{iws} + 2\nu_{ipw} + \nu_{oop}$	3312.5	5.8
194	$2\nu_{ipw} + \nu_{iOH} + \nu_{oop}$	3382.8	0.52
201	$\nu_{ipw} + 2\nu_{oop}$	3433.3	−2.7
204	$3\nu_{oop}$	3451.2	−0.82
255	ν_{fOH}	3691.2	0.29

4.1 Vibrational assignments

The first two lowest-energy vibrational fundamentals of $F^-(H_2O)$, ν_{iws} and ν_{ipw}, are at 424 cm^{-1} and 561 cm^{-1}, respectively. ν_{iws} decreases only slightly to 387 cm^{-1}, while ν_{ipw} decreases significantly, to 407 cm^{-1} for $F^-(D_2O)$. The vibrational band origins (VBOs) characterized as iws and ipw, as well as their combination bands, have been assigned for $F^-(H_2O)$ ($F^-(D_2O)$) up to 8(6) and 5(5) quanta of excitation, respectively. At lower energies, the standard rule of summing the wavenumbers holds well for these vibrations.

VBOs belonging to the oop motion have been assigned with up to three quanta of excitation. The oop fundamental is separated from the rest of the fundamentals by symmetry, which makes it easier to assign combination bands containing the oop motion. Above the 110th vibrational state, the assigned states are almost exclusively ν_{oop} combination bands. The ν_{oop} VBO decreases the most, almost 30%, upon deuteration, from 1181 to 843 cm^{-1}.

The next two fundamentals, ν_{iOH} and ν_{wb}, are found at 1478 and 1634 cm^{-1}, respectively. Their deuterated counterparts come at 1189 and 1215 cm^{-1}, respectively. Several combination bands and the $2\nu_{iOH}$ and $2\nu_{wb}$ overtones have also been identified. The combination bands of these motions are very difficult to assign due to the very strong coupling upon excitation. This coupling already appears for the fundamentals, and it is already extremely strong for the first few combination bands in the 2000 to 2200 cm^{-1} region. For these motions, the standard rule that the wavenumber of a combination mode is simply the sum of the two simple modes is clearly not applicable. The highest-lying vibrational fundamental, ν_{fOH}, is found in our computations at 3691 cm^{-1} for $F^-(H_2O)$.

4.2 Comparison with previous results

Selected vibrational energies of $F^-(H_2O)$ are listed in Table 7, obtained both with the ElVibRot and GENIUSH codes, and compared with their previously determined experimental[7,10,13] and theoretical[9,14,16] counterparts. Agreement between the computed ElVibRot and GENIUSH wavenumbers is excellent,

Table 6 The first 100 vibrational energy levels of the $F^-(D_2O)$ complex and the maximum values of the tunneling splittings of the formally degenerate pairs. The splitting is defined as the difference between the antisymmetric and symmetric state energy levels, $E_{antisym} - E_{sym}$. All values are in cm^{-1}

No.	Label	Energy	Splitting
1	ZPVE	3594.0	1.1×10^{-6}
3	ν_{iws}	387.1	1.3×10^{-6}
5	ν_{ipw}	407.1	1.4×10^{-5}
7	$2\nu_{iws}$	761.0	1.6×10^{-6}
9	$\nu_{iws} + \nu_{ipw}$	788.1	1.4×10^{-5}
11	$2\nu_{ipw}$	806.2	1.3×10^{-5}
13	ν_{oop}	842.9	1.1×10^{-6}
15	$3\nu_{iws}$	1120.5	1.6×10^{-6}
17	$2\nu_{iws} + \nu_{ipw}$	1155.2	2.1×10^{-5}
19	$\nu_{iws} + 2\nu_{ipw}$	1173.2	2.4×10^{-4}
21	ν_{iOH}	1189.3	1.7×10^{-5}
23	$3\nu_{ipw}$	1200.5	3.0×10^{-4}
25	$\nu_{iws} + \nu_{oop}$	1209.3	1.1×10^{-6}
27	ν_{wb}	1215.4	1.0×10^{-5}
29	$\nu_{ipw} + \nu_{oop}$	1246.0	1.8×10^{-5}
31	$4\nu_{iws}$	1470.4	2.2×10^{-6}
33	$3\nu_{iws} + \nu_{ipw}$	1510.3	2.3×10^{-4}
35	$2\nu_{iws} + 2\nu_{ipw}$	1531.6	4.1×10^{-3}
37	$\nu_{iws} + 3\nu_{ipw}$	1552.0	6.5×10^{-3}
39	$2\nu_{iws} + \nu_{oop}$	1565.1	1.2×10^{-6}
41	$\nu_{iws} + \nu_{wb}$	1578.5	1.3×10^{-3}
43	$4\nu_{ipw}$	1587.2	4.5×10^{-3}
45	$\nu_{iws} + \nu_{ipw} + \nu_{oop}$	1604.7	2.2×10^{-5}
47	$\nu_{ipw} + \nu_{iOH}$	1605.7	6.3×10^{-4}
49	$\nu_{ipw} + \nu_{wb}$	1622.0	1.1×10^{-4}
51	$2\nu_{ipw} + \nu_{oop}$	1641.6	7.1×10^{-5}
53	$2\nu_{oop}$	1663.3	7.7×10^{-6}
55	$\nu_{iws} + \nu_{iOH}$	1736.3	6.3×10^{-5}
57	$5\nu_{iws}$	1810.3	2.1×10^{-5}
59	$4\nu_{iws} + \nu_{ipw}$	1853.7	4.0×10^{-3}
61	$3\nu_{iws} + 2\nu_{ipw}$	1875.4	0.075
63	$2\nu_{iws} + 3\nu_{ipw}$	1896.3	0.100
65	$3\nu_{iws} + \nu_{oop}$	1909.0	1.6×10^{-6}
67	$\nu_{iws} + 4\nu_{ipw}$	1924.3	0.100
69	$2\nu_{iws} + \nu_{ipw} + \nu_{oop}$	1953.6	8.5×10^{-5}
71	$5\nu_{ipw}$	1960.0	0.060
73	$2\nu_{iws} + \nu_{wb}$	1968.6	8.1×10^{-3}
75	$2\nu_{ipw} + \nu_{iOH}$	1985.6	0.010
77	$\nu_{iws} + 2\nu_{ipw} + \nu_{oop}$	1987.9	1.0×10^{-3}
79	$\nu_{iws} + \nu_{ipw} + \nu_{wb}$	1997.9	6.4×10^{-3}
81	$\nu_{iws} + 2\nu_{oop}$	2018.8	7.6×10^{-4}
83	$\nu_{oop} + \nu_{iOH}$	2025.1	4.2×10^{-4}
85	$2\nu_{ipw} + \nu_{wb}$	2028.2	1.8×10^{-3}
87	$3\nu_{ipw} + \nu_{oop}$	2030.7	1.7×10^{-3}
89	$\nu_{ipw} + 2\nu_{oop}$	2061.0	7.9×10^{-4}
91	$\nu_{ipw} + \nu_{oop} + \nu_{iOH}$	2076.3	9.5×10^{-6}
93	$6\nu_{iws}$	2123.0	6.8×10^{-4}
95	$\nu_{iws} + \nu_{ipw} + \nu_{iOH}$	2127.1	0.010
97	$2\nu_{iOH}$	2148.2	3.5×10^{-3}
99	$5\nu_{iws} + \nu_{ipw}$	2182.7	0.038

in all cases GENIUSH produces the lower values. In general, the agreement of the present first-principles vibrational energies with their experimental counterparts is quite reasonable. This emphasizes the importance of treating electron correlation at a sufficiently high level of electronic structure theory, as well as that of basis set flexibility and the size of the grid to properly describe the PES of anionic systems with ionic hydrogen bonds.

As to the comparison of the vibrational energies with previous first-principles results,[9,14,16] the agreement is generally acceptable. The values of Kamarchik *et al.*[16] are generally lower than those of Toffoli *et al.*,[14] since they are based on a full-dimensional PES. Although the qualitative agreement is good, some of our variationally computed levels differ significantly from the results of the less accurate VCI computations.

The most intense bands in the IR spectrum of the $F^-(H_2O)$ complex correspond to the fundamental and the first overtone of the iOH stretching mode, observed at about 1500 and 2900 cm^{-1}, respectively. These characteristic bands are strongly anharmonic and reveal the peculiar nature of the $F^-(H_2O)$ cluster as compared to other $X^-(H_2O)$ clusters, already mentioned in the Introduction. In Table 7, ν_{iOH} appears at about the same energy as the previous experimental and theoretical results. The experimental data about the IRPD spectra of $F^-(H_2O)$, given in Table 7, have mainly been obtained from low-resolution time-of-flight photofragmentation measurements. Ayotte *et al.*[7] observed a strong triplet near 2930 cm^{-1}, and assigned it to the double excitation of the ionic OH stretching mode. The present estimate for this mode deviates from this value by almost 100 cm^{-1}. The agreement with the results of Horvath *et al.*[13] is considerably better. Ayotte *et al.*[7] and Roscioli *et al.*[10] observed the free OH stretching mode at 3690 and 3687 cm^{-1}, respectively, in perfect agreement with the present computation.

Comparison of the harmonic and anharmonic vibrational energies (Tables 2 and 7) of $F^-(H_2O)$ reveals large, sometimes very large, differences, resulting from strong anharmonicities, characteristic of this system. The ν_{iOH} fundamental at about 1478 cm^{-1} is considerably lower than the harmonic value, at about 2277 cm^{-1}. Thus, this mode shifts below that of the bending fundamental of the water monomer, 1595 cm^{-1}.[55] Incidentally, the bending fundamental ν_{wb} increases to 1634 cm^{-1} in the $F^-(H_2O)$ anion. Resonances involving $2\nu_{iOH}$ could be behind the different experimental values reported for the overtone of the iOH mode (Table 7).

The results of Table 7 enable us to discuss the tentative assignments of Horvath *et al.*[13] at around 1200, 2200, and 2600 cm^{-1}. The $3\nu_{iws}$ overtone is computed at 1204 cm^{-1}, in agreement with the analysis of Horvath *et al.* The situation is, however, much more complicated around 2200 and 2600 cm^{-1}. The accurate results of the present study suggest that $(\nu_{iws} + \nu_{iOH})$ is at about 2020 cm^{-1}, some 100 cm^{-1} lower than predicted by Horvath *et al.*, while $(2\nu_{iws} + \nu_{iOH})$ is around 2546 cm^{-1}, in better agreement with the experimental predictions. Vibrational energies with different labels have been found around 2200 cm^{-1}: these are the resonating $4\nu_{ipw}$ and $(2\nu_{ipw} + \nu_{iOH})$ states. The first overtone of the out-of-plane mode is also in this energy range at 2335 cm^{-1}. The cut of the PES along the r_2 and R coordinates, see Fig. 4, confirms that this part of the potential is strongly anharmonic.

Horvath *et al.*[13] measured two experimental bands for $F^-(D_2O)$. The fundamental and the first overtone of the ionic OH stretching, ν_{iOH} and $2\nu_{iOH}$, respectively, were found in the region of 1160–1270 cm^{-1} and 2120–2263 cm^{-1}, respectively. They are in reasonable agreement with our theoretical results, 1189.3 cm^{-1} and 2148.2 cm^{-1}, respectively.

4.3 Tunneling splittings

As computations involving the Eckart–Watson Hamiltonian[56,57] are performed with the reference, defining the normal modes,

Table 7 Selected variationally computed vibrational energy levels, in cm^{-1}, of $F^-(H_2O)$ compared to previous experimental and theoretical results. Description of the labels used can be found in Table 2

Labels	Expt.[7]	Expt.[10]	Expt.[13]	Ref. 9	Ref. 14	Ref. 16	GENIUSH	ElVibRot[b]
ZPVE							4831.0	4831.0
ν_{iws}				431	426.7	433.2	423.5	423.5
ν_{ipw}				581	576.3	566.6	560.7	560.8
$2\nu_{iws}$				836	829.1	836.9	823.3	823.3
$2\nu_{ipw}$				1129	1200.8	1169.8	1110.4	1110.6
ν_{oop}		1083–1250		1166	1184.4	1146.6	1180.7	1181.0
$3\nu_{iws}$			1200[a]		1218.0	1219.9	1203.7	1203.7
ν_{iOH}		1523	1430–1570	1488	1464.5	1456.7	1477.9	1478.2
ν_{wb}		1650		1645	1653.6	1623.3	1634.4	1634.8
$\nu_{iws} + \nu_{iOH}$			2200[a]				2020.3	2020.9
$2\nu_{oop}$				2314	2352.4	2314.6	2332.2	2332.6
$2\nu_{iws} + \nu_{iOH}$			2600[a]		2634.7	2561.4	2546.0	
$2\nu_{iOH}$	2930	2905(20)	2815–2930	2888	2915.9	2872.5	2837.3	
$2\nu_{wb}$				3265	3281.9	3225.5	3213.4	
ν_{fOH}	3690	3687		3640	3689.0	3660.7	3691.2	3691.0

[a] Tentative assignment. [b] ElVibRot levels obtained with $L_B = 7$ and $L_G = 8$ (see text).

set as one of the two equivalent C_{2v} minima, no tunneling splittings can be computed with this approach. The splittings presented in Tables 4–6 have not been determined before.

Even for $F^-(H_2O)$, the first few tunneling splittings are minuscule, for the ground vibrational state the splitting is smaller than 8×10^{-7} cm^{-1} and it remains below 0.01 cm^{-1} for about the first 20 vibrational states. Upon vibrational excitation, especially including the tunneling motion, ipw, the splitting increases quickly and reaches 1 cm^{-1} around the 41st vibrational state, $\nu_{iws} + 3\nu_{ipw}$. Nevertheless, many higher-lying states containing only a small contribution from ipw have very small splittings. For example, the splitting of the 134th state, with the label of $2\nu_{iws} + 2\nu_{oop}$, has a splitting of only 1.6×10^{-3} cm^{-1}.

Table 8 The $J = 1$ and $J = 2$ rovibrational energy levels, in cm^{-1}, of the first six and three VBOs of $F^-(H_2O)$, respectively, computed with GENIUSH, showing only the lower-energy component of each tunneling pair. The values are compared to the rigid rotor (RR) energy levels

VBO	K	RR	VAR
$J = 1$			
ν_{ZP}	0	0.62	0.63
	1	20.41	20.90
	−1	20.41	20.90
ν_{iws}	0	0.62	0.61
	1	20.41	20.80
	−1	20.41	20.80
ν_{ipw}	0	0.62	0.63
	1	20.41	21.58
	−1	20.41	21.59
ν_{oop}	0	0.62	0.62
	1	20.41	18.46
	−1	20.41	18.46
ν_{iOH}	0	0.62	0.63
	1	20.41	21.51
	−1	20.41	21.51
ν_{wb}	0	0.62	0.64
	1	20.41	23.19
	−1	20.41	23.24
$J = 2$			
ν_{ZP}	0	1.86	1.88
	1	21.65	22.14
	−1	21.65	22.16
	2	81.04	82.85
	−2	81.04	82.85
ν_{iws}	0	1.86	1.84
	1	21.65	22.02
	−1	21.65	22.03
	2	81.04	82.46
	−2	81.04	82.46
ν_{ipw}	0	1.86	1.87
	1	21.65	22.81
	−1	21.65	22.84
	2	81.04	85.48
	−2	81.04	85.48

The splitting corresponding to the $4\nu_{ipw}$ states is sizable, 2.2 cm^{-1}. These ipw splittings basically confirm the 1D study of Kamarchik *et al.*[16] along the MEP. The results are consistent with those of Wang and Carrington[17] for the $Cl^-(H_2O)$ anionic complex, who obtained considerably larger splittings and a steady increase of the splittings for the excited ipw modes. Wang and Carrington obtained a splitting of 0.35 cm^{-1} for the vibrational ground state, which quickly increases with the number of excitations to 228 cm^{-1} by the $5\nu_{ipw}$ state. The larger splittings for $Cl^-(H_2O)$ are related to the lower and narrower transition barrier between the C_s minima. To wit, the barrier height is 640 cm^{-1} in $Cl^-(H_2O)$ to be compared with 2500 cm^{-1} in $F^-(H_2O)$.

Upon deuteration, one would expect the whole tunneling process to come to an almost complete halt. For $F^-(D_2O)$, the tunneling splitting of the vibrational ground state is indeed orders of magnitude smaller than for $F^-(H_2O)$. More significantly, the tunneling splittings mostly remain below 10^{-3} cm^{-1} for the first 100 vibrational states. The excitation of the tunneling motion, similarly to $F^-(H_2O)$, increases the splitting, which goes up to 0.1 cm^{-1} for the $2\nu_{iws} + 3\nu_{ipw}$ state.

4.4 Rovibrational states

The rovibrational states of $F^-(H_2O)$ were studied only with GENIUSH. The computed $J = 1$ and $J = 2$ states, 99 and 165, respectively, correspond to the rotational levels of the first 33 vibrational states. Comparison of the rovibrational energies to their rigid-rotor (RR) model counterparts shows excellent agreement (see Table 8).

5 Conclusions

A new six-dimensional potential energy surface, called the SLBCL PES, is determined for the $F^-(H_2O)$ anionic cluster using the CCSD(T)-F12a methodology of electronic structure theory and a large Gaussian basis set. The PES describes the two equivalent C_s minima and the connecting C_{2v} transition state of the system, and two low-energy dissociation pathways, $F^-(H_2O) \rightarrow F^- + H_2O$ and $F^-(H_2O) \rightarrow HF + OH^-$. Most of the peculiar characteristics of the $O\cdots H\cdots F^-$ proton transfer process are also well reproduced. Several regions of the PES are strongly anharmonic: most of the normal modes change strongly between the transition state and the two equivalent minima.

In order to compute the vibrational energies of the complex accurately, the ElVibRot variational nuclear-motion code has been improved, allowing the use of curvilinear coordinates corresponding to a reaction path. The use of such coordinates facilitates the description of strongly coupled internal motions, like the tunneling motion in $F^-(H_2O)$, and the strong coordinate variations along an arbitrary path. This procedure is fully general and it enables to deal with reactions, including isomerizations, described with more than one elementary active internal coordinate. This approach is similar in spirit to the Reaction Surface Hamiltonian approach,[40] where two active coordinates are used.

The highly similar ElVibRot and GENIUSH results reveal the presence of strong resonances, especially pronounced for the ν_{wb} and $2\nu_{iOH}$ states. For many states the anharmonic corrections, defined as the difference between the energies of the anharmonic and harmonic vibrational energies, are particularly large. These large differences are due not only to the existence of strongly anharmonic regions of the potential energy surface but also to strong coordinate couplings.

Agreement of the present vibrational energies and their assignment with previous experimental and theoretical works is reasonable for most bands. Many of the vibrational states of $F^-(H_2O)$, and similarly of $F^-(D_2O)$, are difficult to label due to the presence of strong resonances.

The authors are grateful to the COST action ''Molecules in Motion'' (MOLIM, CM1405) for support. The authors would like to thank J. M. Bowman and S. Carter for fruitful discussions and advice. JS and AGC thank the NKFIH (grant number NK83583) for supporting the work performed in Hungary.

References

1 M. Meot-Ner (Mautner), *Chem. Rev.*, 2012, **112**, PR22–PR103.
2 M. D. Joesten and L. J. Schaad, *Hydrogen Bonding*, Marcel Dekker, New York, 1974.
3 J. Emsley, *Chem. Soc. Rev.*, 1980, **9**, 91–124.
4 J. W. Larson and T. B. McMahon, *J. Am. Chem. Soc.*, 1983, **105**, 2944–2950.
5 B. F. Yates, H. F. Schaefer III, T. J. Lee and J. E. Rice, *J. Am. Chem. Soc.*, 1988, **110**, 6327–6332.
6 N. E. Klepeis, A. L. L. East, A. G. Császár, W. D. Allen, T. J. Lee and D. W. Schwenke, *J. Chem. Phys.*, 1993, **99**, 3865–3897.
7 P. Ayotte, J. A. Kelley, S. B. Nielsen and M. A. Johnson, *Chem. Phys. Lett.*, 2000, **316**, 455–459.
8 J. Kim, H. M. Lee, S. B. Suh, D. Majumdar and K. S. Kim, *J. Chem. Phys.*, 2000, **113**, 5259–5272.
9 G. M. Chaban, S. S. Xantheas and R. B. Gerber, *J. Phys. Chem. A*, 2003, **107**, 4952–4956.
10 J. R. Roscioli, E. G. Diken, M. A. Johnson, S. Horvath and A. B. McCoy, *J. Phys. Chem. A*, 2006, **110**, 4943–4952.
11 K. D. Collins, G. W. Neilson and J. Enderby, *Biophys. Chem.*, 2007, **128**, 95–104.
12 J. R. Roscioli, L. R. McCunn and M. A. Johnson, *Science*, 2007, **316**, 249–254.
13 S. Horvath, A. B. McCoy, J. R. Roscioli and M. A. Johnson, *J. Phys. Chem. A*, 2008, **112**, 12337–12344.
14 D. Toffoli, M. Sparta and O. Christiansen, *Chem. Phys. Lett.*, 2011, **510**, 36–41.
15 Q. Wang, K. Suzuki, U. Nagashima, M. Tachikawa and S. Yan, *J. Theor. Appl. Phys.*, 2013, **7**, 7.
16 E. Kamarchik, D. Toffoli, O. Christiansen and J. M. Bowman, *Spectrochim. Acta, Part A*, 2014, **119**, 59–62.
17 X.-G. Wang and T. Carrington Jr., *J. Chem. Phys.*, 2014, **140**, 204306.
18 O. Christiansen, *J. Chem. Phys.*, 2004, **120**, 2149–2159.
19 J. Rheinecker and J. M. Bowman, *J. Chem. Phys.*, 2006, **124**, 131102.
20 D. Lauvergnat, ElVibRot Quantum Dynamics Code, http://www.lcp.u-psud.fr/Pageperso/lauvergnat/ElVibRot.html.
21 E. Mátyus, G. Czakó and A. G. Császár, *J. Chem. Phys.*, 2009, **130**, 134112.
22 C. Fábri, E. Mátyus and A. G. Császár, *J. Chem. Phys.*, 2011, **134**, 074105.
23 C. Fábri, E. Mátyus and A. G. Császár, *Spectrochim. Acta A*, 2014, **119**, 84–89.
24 H.-J. Werner, T. B. Adler and F. R. Manby, *J. Chem. Phys.*, 2007, **126**, 164102.
25 G. Knizia, T. B. Adler and H.-J. Werner, *J. Chem. Phys.*, 2009, **130**, 054104.
26 V. Brites and C. Léonard, *Int. J. Quantum Chem.*, 2012, **112**, 2051–2061.
27 V. Brites and L. Jutier, *J. Mol. Spectrosc.*, 2012, **271**, 25–32.
28 V. Brites and C. Léonard, *Mol. Phys.*, 2011, **109**, 2655–2662.
29 T. B. Adler, G. Knizia and H.-J. Werner, *J. Chem. Phys.*, 2007, **127**, 221106.
30 A. G. Császár and W. D. Allen, *J. Chem. Phys.*, 1996, **104**, 2746–2748.
31 H.-J. Werner, P. J. Knowles, R. Lindh, F. R. Manby, M. Schütz, *et al., MOLPRO, version 2010.1*, a package of *ab initio* programs.
32 K. A. Peterson, T. B. Adler and H.-J. Werner, *J. Chem. Phys.*, 2008, **128**, 084102.
33 J. Grant Hill, S. Mazumder and K. A. Peterson, *J. Chem. Phys.*, 2010, **132**, 054108.
34 C. Hättig, *Phys. Chem. Chem. Phys.*, 2005, **7**, 59–66.

35 C. Blondel, C. Delsart and F. Goldfarb, *J. Phys. B: At., Mol. Opt. Phys.*, 2001, **34**, L281–L288, 2757 (erratum).
36 See the ESI† for additional information regarding (I) details on the parameters of the PES applied; (II) Complete list of the computed vibrational energy levels for $F^-(H_2O)$.
37 D. Lauvergnat and A. Nauts, *J. Chem. Phys.*, 2002, **116**, 8560–8570.
38 D. Lauvergnat and A. Nauts, *Spectrochim. Acta, Part A*, 2014, **119**, 18–25.
39 W. H. Miller, N. C. Handy and J. E. Adams, *J. Chem. Phys.*, 1980, **72**, 99–112.
40 T. Carrington Jr. and W. H. Miller, *J. Chem. Phys.*, 1984, **81**, 3942–3950.
41 R. Meyer and H. H. Günthard, *J. Chem. Phys.*, 1969, **50**, 353–365.
42 J. T. Hougen, P. R. Bunker and J. W. C. Johns, *J. Mol. Spectrosc.*, 1970, **34**, 136–172.
43 D. Lauvergnat and A. Nauts, *Chem. Phys.*, 2004, **305**, 105–113.
44 Y. Scribano, D. Lauvergnat and D. M. Benoit, *J. Chem. Phys.*, 2010, **133**, 094103.
45 E. B. Wilson Jr. and J. Howard, *J. Chem. Phys.*, 1936, **4**, 260–268.
46 E. R. Davidson, *J. Comput. Phys.*, 1975, **17**, 87–94.
47 F. Ribeiro, C. Iung and C. Leforestier, *Chem. Phys. Lett.*, 2002, **362**, 199–204.
48 R. Dawes and T. Carrington Jr., *J. Chem. Phys.*, 2005, **122**, 134101.
49 S. A. Smolyak, *Sov. Math. Dokl.*, 1963, **4**, 240–243.
50 G. Avila and T. Carrington, *J. Chem. Phys.*, 2009, **131**, 174103.
51 G. Avila and T. Carrington, *J. Chem. Phys.*, 2011, **135**, 064101.
52 A. G. Császár, C. Fábri, T. Szidarovszky, E. Mátyus, T. Furtenbacher and G. Czakó, *Phys. Chem. Chem. Phys.*, 2012, **14**, 1085–1106.
53 J. C. Light and T. Carrington Jr., *Adv. Chem. Phys.*, 2000, **114**, 263–310.
54 C. Lanczos, *J. Res. Natl. Bur. Stand.*, 1950, 255–282.
55 J. Tennyson, P. F. Bernath, L. R. Brown, A. Campargue, M. R. Carleer, A. G. Császár, L. Daumont, R. R. Gamache, J. T. Hodges, O. V. Naumenko, O. L. Polyansky, L. S. Rothman, A. C. Vandaele, N. F. Zobov, A. R. Al Derzi, C. Fábri, A. Z. Fazliev, T. Furtenbacher, I. E. Gordon, L. Lodi and I. Mizus, *J. Quant. Spectrosc. Radiat. Transfer*, 2013, **117**, 29–80.
56 C. Eckart, *Phys. Rev.*, 1935, **47**, 552–558.
57 J. K. G. Watson, *Mol. Phys.*, 1968, **15**, 479–490.

